LAWRENCE
LIVERMORE
NATIONAL
LABORATORY

LLNL-JRNL-417117

Effect of electrode material and design on sensitivity and selectivity for high temperature impedancemetric NOx sensors

L. Y. Woo, R. S. Glass, R. F. Novak, J. H. Visser

September 24, 2009

Journal of The Electrochemical Society

Disclaimer

This document was prepared as an account of work sponsored by an agency of the United States government. Neither the United States government nor Lawrence Livermore National Security, LLC, nor any of their employees makes any warranty, expressed or implied, or assumes any legal liability or responsibility for the accuracy, completeness, or usefulness of any information, apparatus, product, or process disclosed, or represents that its use would not infringe privately owned rights. Reference herein to any specific commercial product, process, or service by trade name, trademark, manufacturer, or otherwise does not necessarily constitute or imply its endorsement, recommendation, or favoring by the United States government or Lawrence Livermore National Security, LLC. The views and opinions of authors expressed herein do not necessarily state or reflect those of the United States government or Lawrence Livermore National Security, LLC, and shall not be used for advertising or product endorsement purposes.

Effect of electrode material and design on sensitivity and selectivity for high temperature impedancemetric NO_x sensors

Leta Y. Woo[a], Robert S. Glass[a], Robert F. Novak[b], Jaco H. Visser[b]

LLNL-JRNL-417117

[a] *Lawrence Livermore National Laboratory, Livermore, California 94551, USA*

[b] *Ford Motor Company, Dearborn, Michigan 48121, USA*

Abstract

Solid-state electrochemical sensors using two different sensing electrode compositions, gold and strontium-doped lanthanum manganite (LSM), were evaluated for gas phase sensing of NO_x (NO and NO_2) using an impedancemetric technique. An asymmetric cell design utilizing porous YSZ electrolyte exposed both electrodes to the test gas (i.e., no reference gas). Sensitivity to less than 5 ppm NO and response/recovery times (10-90%) less than 10 s were demonstrated. Using an LSM sensing electrode, virtual identical sensitivity towards NO and NO_2 was obtained, indicating that the equilibrium gas concentration was measured by the sensing electrode. In contrast, for cells employing a gold sensing electrode the NO_x sensitivity varied depending on the cell design: increasing the amount of porous YSZ electrolyte on the sensor surface produced higher NO_2 sensitivity compared to NO. In order to achieve comparable sensitivity for both NO and NO_2, the cell with the LSM sensing electrode required operation at a lower temperature (575°C) than the cell with the gold sensing electrode (650°C). The role of surface reactions are proposed to explain the differences in NO and NO_2 selectivity using the two different electrode materials.

Introduction

As the regulation of pollutants becomes increasingly more stringent, the development of advanced gas sensors for use in automotive feedback control systems to reduce emissions are critical.[1–3] Diesel engines offer higher fuel efficiency than gasoline internal combustion engines, but require additional exhaust after-treatment and engine optimization in order to meet emission limits, in particular for NO_x (NO and NO_2) which act as both pollutants and potent greenhouse gases.

The technical performance requirements for NO_x sensors present extreme challenges in terms of stability, accuracy, and sensitivity.[4–6] In addition, for automotive applications, minimizing the cost of the sensor is an important factor. In consideration of these factors, and the requirement for in-situ operation in harsh, high-temperature automotive exhaust environments, solid-state electrochemical sensors are a viable, robust technology (e.g., the oxygen stoichiometric sensor).[2–6] These types of sensors typically rely on yttria-stabilized zirconia (YSZ) as the oxygen-ion conducting electrolyte and then target different types of metal-oxide electrodes to optimize the response.[2–6]

Different modes of operation for electrochemical sensors have been explored, including amperometric and potentiometric, which both employ direct current (dc) measurements. Amperometric operation is costly due to the electronics necessary to measure the small sensor signal (nanoampere

current at ppm NO_x levels), and cannot easily be improved to meet the future technical performance requirements. Potentiometric operation, which uses voltage as the sensor signal, has not shown enough promise in meeting stability requirements for the long lifetimes required (up to 10 years). It is thought that the drift observed is due to aging effects associated with electrically driven changes, both morphological and compositional, in the sensor.[7]

Another approach is impedancemetric operation, which uses alternating current (ac) measurements at a specified frequency.[8–13] Impedancemetric operation has shown the potential to overcome the drawbacks of other approaches, including higher sensitivity towards NO_x, better long-term stability, and lower cost materials.[11–13] The approach is related to solid-state impedance spectroscopy, an electrochemical characterization technique that measures the cell response over a range of frequencies, typically from sub-Hertz to mega-Hertz.[14] The frequency-dependent behavior can be used to identify individual electrochemical components if they have significantly different time constants (e.g., interfacial and bulk phenomena), in which case they can be separated for individual analysis. The electrode impedance or polarization, primarily associated with processes at the electrode/electrolyte interface, dominates the low-frequency regime, typically at less than 1 kHz. Only a single frequency is needed for sensor operation.

Previous work by the authors demonstrated the impedance response of

symmetric Au/YSZ/Au cells to NO_x.[12] Subsequent work focused on the role of electrode composition and microstructure and provided criteria for higher sensitivity electrodes, which depended on limiting the oxygen reaction on the electrode so that the NO_x reaction could be resolved.[13] Our previous work suggested that impedancemetric sensing was possible with a variety of electrode materials that meet some general sensor criteria, which include a dense microstructure and appropriate composition to limit the catalytic activity towards oxygen.[13]

Previous work focused on metal sensing electrodes, and dense gold was found to produce the largest NO_x sensitivity compared with silver and platinum.[13] However, the low melting temperature of gold requires a separate, lower temperature processing step. In contrast, metal-oxide electrodes would be more desirable from a processing flexibility standpoint since the metal-oxide electrodes and YSZ electrolyte could be co-fired in a single firing step. Metal-oxide electrodes may also provide better long-term thermal and mechanical stability because of higher melting temperatures and better thermal expansion match with the YSZ electrolyte.

For an electrochemical cell with two electrodes, impedancemetric sensing requires that at least one of the electrodes act as the "sensing" electrode. The sensing electrode will have a preferable response to NO_x over other gas phase components. However, in impedancemetric sensing, both electrodes can have an appreciable response. Therefore, the sensor design is flexible

and can either contain one sensing electrode and one counter (i.e., non-sensing) electrode, or two sensing electrodes. In this study, the impedancemetric sensing performance of two sensing electrode compositions, gold and a metal oxide, are compared using asymmetric cell designs that included one sensing electrode and a second counter (i.e., non-sensing) electrode. The properties of the sensing electrode materials, gold wire metal and dense sintered strontium-doped lanthanum manganite (LSM), put different constraints on cell design. While similar overall NO_x sensitivity was observed for the different designs, differences in NO and NO_2 selectivity were noted. The influence of specific cell design characteristics on surface reactions are proposed to explain the latter.

Experimental

Two different cell designs were investigated. The first utilized a Au wire sensing electrode and a Pt counter electrode. The counter electrode was formed by painting a Pt ink (Engelhard 6082) onto a dense alumina substrate (10 mm $\times$ 10 mm $\times$ 0.5 mm, 99.6% Alumina, Valley Design Corp.), which was then fired at 1200°C. The design demonstrated the feasibility for incorporating a self-heated substrate in future designs, which typically consists of an alumina substrate with a Pt resistive heating element. A slurry of yttria-stabilized zirconia (YSZ) powder (Tosoh Corp., 8 mol% Y_2O_3-doped ZrO_2) mixed with ethanol, binder (polyvinyl butyral, Butvar), dispersant

(phosphate ester), and plasticizer (dipropylene glycol dibenzoate) was then coated onto the fired Pt. Au wire sensing electrodes (0.25 mm diameter, Alfa Aesar) were then attached to the surface of the YSZ electrolyte and secured by applying additional YSZ slurry, in sequential layers (up to four) on top of the wires. The assembly was then fired at 1000°C. A schematic of the resulting Pt/YSZ/Au cell is shown in Fig. 1a.

The Au wire sensing electrode also served as an external lead for electrical measurements, and a second Au wire was attached to the Pt counter electrode with Au paste (8880-G, ElectroScience Laboratory) to serve as the other external lead.

The second cell used a strontium-doped lanthanum manganite (LSM) sensing electrode. The cell was fabricated using a LSM pellet. To make the pellet $(La_{0.85}Sr_{0.15})_{0.98}MnO_3$ powder (Praxair) was pressed in a uniaxial die and then sintered at 1400°C for 6 h. The sintered pellet (> 95% theoretical density) served as the sensing electrode and had a diameter of 11 mm with a thickness of ∼1.5 mm. To deposit the electrolyte the LSM pellet was dip-coated with YSZ slurry and fired at 1000°C. A slurry made from LSM powder mixed with organic binder (V-006, Heraeus) was coated on the YSZ electrolyte and fired to 1000°C to produce a porous LSM counter electrode. A schematic of the resulting LSM/YSZ/LSM_{porous} electrochemical cell is shown in Fig. 1b. External leads for electrical measurements were made by attaching Au wires using Au paste. This design demonstrated the use of

only high-temperature cell materials, which may simplify processing steps and further improve long-term stability.

Gas sensing experiments were performed in a quartz tube (21.4 mm I.D.) placed inside a tube furnace with both electrodes exposed to the same gaseous environment. The gas flow rate was maintained at 500 ml/min with the composition controlled by mixing air, N_2, 1000 ppm NO in N_2, and 1000 ppm NO_2 in N_2 using a standard gas handling system equipped with thermal mass flow controllers. All gas compositions contained approximately 1% water vapor, which was introduced by flowing 450 ml/min mixtures of air and N_2 through a water bubbler while the remaining 50 ml/min of the gas mixture contained dry mixtures of N_2, NO, and NO_2 to prevent NO_x from dissolving in the water.

Gas sensing measurements for the Pt/YSZ/Au cell were performed at 650°C. For the LSM/YSZ/LSM_{porous} cell the gas sensing measurements were performed at 575°C.

Electrochemical measurements were performed using a Solartron Analytical SI 1260 Impedance/gain-phase analyzer with the Solartron Analytical SI 1287 electrochemical interface. Computer-controlled data acquisition used the commercially available ZPlot and CorrWare software (Scribner Associates, Inc.). Impedance spectra were obtained using an excitation voltage of 25 mV over the frequency range 1 MHz to 1 Hz at 10 steps per frequency decade. Current-voltage (I-V) measurements were made over the potential

range -25 to 25 mV.

Results and Discussion

Impedancemetric sensing

The impedance of a material (Z) describes the electrical response to an alternating signal, and includes both magnitude ($|Z|$) and phase angle (θ) information. The following relationships describe the complex impedance ($Z(\omega) = \mathrm{Re}(Z) + j\mathrm{Im}(Z)$), where $\mathrm{Re}(Z)$ is the real component and $\mathrm{Im}(Z)$ is the imaginary component:[14]

$$\mathrm{Re}(Z) = |Z|\cos\theta \quad \text{and} \quad \mathrm{Im}(Z) = |Z|\sin\theta \tag{1}$$

The relationship for phase angle is described by the following:

$$\theta = \tan^{-1}\left(\frac{\mathrm{Im}(Z)}{\mathrm{Re}(Z)}\right) \tag{2}$$

and for the magnitude:

$$|Z| = \sqrt{(\mathrm{Re}(Z))^2 + (\mathrm{Im}(Z))^2} \tag{3}$$

For impedancemetric sensor operation, a sensing signal (e.g., $\mathrm{Re}(Z)$, $\mathrm{Im}(Z)$, θ, or $|Z|$) is chosen at a specified frequency.[8–13] Figure 2 shows the Nyquist plot (complex plane representation of -$\mathrm{Im}(Z)$ vs. $\mathrm{Re}(Z)$) for the Pt/YSZ/Au cell at 650°C in 10.5% O_2 and in 10.5% O_2 with 100 ppm NO or 100 ppm NO_2. Each datum is taken at a different frequency, increasing from right to left, where the numbers corresponding to darkened points

represent log of frequency in Hz. Features in the Nyquist plot, in particular the semicircular arcs, can be used to determine the contributions from interfacial and bulk phenomena to the overall impedance. The diameter of the individual arcs corresponds to real impedance (resistance) values.

In Fig. 2, the addition of either NO or NO_2 causes a decrease in the Pt/YSZ/Au cell impedance over the frequency range less than about 1 kHz, with NO_2 causing a slightly larger decrease in impedance than NO. At frequencies higher than about 10 kHz, the addition of NO_x has no apparent effect. Changes in impedance for frequencies less than 1 kHz are often associated with electrode impedance and are influenced by reactions at the interface between the electrode and electrolyte. At higher frequencies, the impedance behavior is dominated by changes in bulk conductivity (e.g., the conductivity through the ionic conductor).

Practical sensor operation requires that measurements be obtained at a selected frequency. Previous work by Miura et al. on impedance-based NO_x gas sensors used the magnitude ($|Z|$) at 1 Hz.[8,10] The frequency of operation is chosen as a tradeoff between the increased sampling rate (i.e., signal-to-noise ratio) at higher frequencies and the increased sensitivity at lower frequencies.[11] Previous work by our group has found excellent sensitivity at frequencies as high as 10 Hz.[11–13] In Fig. 2, both the $|Z|$ and θ at 10 Hz are highlighted for measurements made in 10.5% O_2 and in 10.5% O_2 with 100 ppm of NO or 100 ppm NO_2 (approximately equivalent response).

Clearly it is possible to make measurements of NO_x at these levels (and below) using either $|Z|$ or θ at this frequency.

Figures 3a and b show the NO sensing behavior using four different measurement signals (i.e., Re(Z), Im(Z), θ, or $|Z|$) at 10 Hz for the Pt/YSZ/Au cell at 650°C in 10.5% O_2. In this figure, the NO concentration was changed from baseline to 20 ppm, stepped in 5 ppm increments back to 0 ppm, then increased again. The 5 ppm changes are clearly resolved with similar sensitivities, signal-to-noise ratios, and response/recovery times (10-90%) of less than 10 s for all four measurement signals. Previous work has shown that the θ signal generally produced better sensitivity and higher signal-to-noise ratio than the $|Z|$ at higher frequencies.[11]

Figure 4 shows the Nyquist plot for the LSM/YSZ/LSM_{porous} cell at 575°C in 10.5% O_2 and in 10.5% O_2 with 100 ppm NO or 100 ppm NO_2. Similar to the behavior shown in Fig. 2 for the Pt/YSZ/Au cell at 650°C, Fig. 4 shows that the addition of either NO or NO_2 changes the lower frequency (less than about 1 kHz) impedance, but does not alter the higher frequency (higher than about 10 kHz) response, which is shown in the inset. However, in contrast to the Pt/YSZ/Au cell where the addition of NO_2 caused slightly larger changes than NO, Fig. 4 shows that the addition of either NO or NO_2 produces nearly identical impedance response.

Figure 5a and b show measurements made using Re(Z), Im(Z), θ, or $|Z|$ at 10 Hz for the LSM/YSZ/LSM_{porous} cell at 575°C in 10.5% O_2 using

a similar strategy for varying the NO concentration as that described in Fig. 3. However, in contrast to the Pt/YSZ/Au cell at 650°C, only the phase angle signal (θ) is able to clearly resolve 5 ppm changes in NO with response/recovery times (10-90%) of less than 10 s. Furthermore, Fig. 6 shows that the measurement sensitivity using the phase angle signal at 10 Hz is simlar for the Pt/YSZ/Au cell at 650°C and for the LSM/YSZ/LSM$_{porous}$ cell at 575°C, approximately 0.07 and 0.06 degrees/ppm NO, respectively.

The role of electrolyte and electrode surface reactivity on NO$_x$ sensitivity and selectivity

For gaseous environments containing both O_2 and NO_x, the following redox reactions may occur at the triple point between the electrode, electrolyte, and gas phase:

$$\frac{1}{2}O_2 + 2e^- \rightleftharpoons O^{2-} \tag{4}$$

$$NO_2 + 2e^- \rightleftharpoons NO + O^{2-} \tag{5}$$

In our previous work, sensitivity was found to rely on parallel contributions from the NO_x and O_2 reactions occurring at the sensing electrode/electrolyte interface.[12,13] Whether NO_x can be detected at ppm levels in the much larger background O_2 concentration (2 to 18.9 %) is dependent upon the magnitudes of the rate constants for the rate-determining step(s) for the O_2 reaction. Electrodes with dense microstructures and compositions that have low catalytic activity towards O_2 will minimize the rela-

tive contribution of the O_2 reaction and produce higher NO_x sensitivity in impedancemetric sensors.[13]

Figure 7 illustrates the impedancemetric NO_x sensing mechanisms using simplified steps for the electrochemical redox reactions. The actual redox reactions likely involve a more complex series of steps (e.g., adsorption of gas species, transport along surfaces, electron transfer, diffusion of products away from reaction sites, etc.). In the case of low NO_x sensitivity (Fig. 7a), if adsorption and diffusion on the electrode predominates, the NO_x reaction rate will not be able to compete with the O_2 reaction rate in a much larger backgound of O_2, and impedance changes associated with ppm variations in NO_x are not resolved. In the case of high NO_x sensitivity (Fig. 7b), there are fewer reaction sites on electrodes with low activity (i.e., dense microstructures and compositions that do not interact with O_2) and reaction sites on the electrolyte begin to dominate the measured impedance.

When the contribution from reaction pathways on the electrolyte increases relative to the contribution from the electrode, changes associated with ppm variation in NO_x are resolved. The YSZ electrolyte surface has previously been shown to be highly active towards NO_x.[15] Yang et al. used temperature-programmed desorption (TPD), diffuse reflectance infrared fourier transform spectroscopy (DRIFTS), and chemical reactivity measurements to show the formation of surface nitrates and demonstrate strong interactions between the NO_x molecules and YSZ.[15]

Both the Pt/YSZ/Au and LSM/YSZ/LSM_{porous} cells are asymmetric with only one sensing electrode, Au and LSM, respectively. Either can be used as a NO_x sensor using the appropriate choice of temperature and response signal (e.g., phase angle θ). This further supports a sensing mechanism where NO_x sensitivity is controlled by processes occurring on the YSZ electrolyte surface.

The difference in operating temperatures necessary to obtain similar NO_x sensitivities for the Au and LSM sensing electrodes can be explained by their differing catalytic activities. LSM is more active towards oxygen catalysis than Au. The catalytic activity of oxides is determined primarily by the binding energy of surface oxygen.[16,17] The catalytic activity of LSM, a perovskite-type oxide, has been shown to depend on preparation and temperature of operation.[18,19] At 650°C, the LSM electrode did not resolve ppm changes in NO_x, unlike the Au electrode at the same temperature, even though both electrodes had similarly dense microstructures. However, reducing the operating temperature of the LSM electrode to 575°C lowers the catalytic activity towards O_2 and enhances NO_x selectivity over O_2, allowing ppm level sensitivity.

The following equation describes the gas phase relationship between O_2, NO, and NO_2:

$$NO_2 \leftrightarrow NO + \frac{1}{2}O_2 \tag{6}$$

and can be used to calculate equilibrium values for NO and NO_2 using ther-

modynamic data for 10.5% O_2. At 575°C and 650°C, the equilibrium NO_x gas mixture has 87% and 93% NO, respectively. For the LSM/YSZ/LSM_{porous} cell, the identical responses to either NO or NO_2 suggest that the equilibrium NO_x concentration is presented at the sensing electrode.

Figure 8 shows the current-potential (I-V) curves for the LSM/YSZ/LSM_{porous} cell at 575°C in 10.5% O_2 and in 10.5% O_2 with 100 ppm NO or 100 ppm NO_2. For ohmic behavior, the slope of the I-V curve in Fig. 8 corresponds to the inverse of the resistance. The I-V curves corresponding to 10.5% O_2 with 100 ppm NO or 100 ppm NO_2 have similar slopes and reflect the decreased resistance/impedance, as compared to the I-V curve corresponding to 10.5% O_2.

In the I-V curves, the potential at zero current, or open circuit potential (OCP), indicates the difference in reaction rates between the two electrodes. When NO_x is present, several electrode reactions occur (see Eqs. 4 and 5) which may produce a nonequilibrium OCP in cells with two different electrode materials (e.g., Au and Pt) exposed to the same test gas.[20,21] Whereas OCP provides a measure of the difference in reaction rates between the two electrodes, impedance measures overall changes in reaction rates at each electrode.

In Fig. 8, an OCP of approximately 2 mV was measured for both 10.5% O_2 and 10.5% O_2 with 100 ppm NO. An OCP of approximately -2 mV was measured for 10.5% O_2 with 100 ppm NO_2. The minimal OCP values with

magnitudes less than about 2 mV indicate a negligible difference in reaction rates between the electrodes and that similar equilibrium gas concentrations are present at both electrodes.

Due to the geometry of the LSM/YSZ/LSM$_{porous}$ cell, the gas interacts with the porous LSM counter electrode before reaching the dense LSM sensing electrode. The interaction with the porous LSM may provide enough catalytic activity for complete gas phase equilibration of NO_x (with equilibrium gas phase composition approximately 87% NO). Therefore, identical equilibrium gas concentrations reach both electrodes, regardless of whether the starting gas is NO or NO_2, and identical responses are produced.

For the Pt/YSZ/Au cell, NO_2 produces a slightly larger response than NO indicating that the equilibrium NO_x concentration is not present at the sensing electrode/YSZ interface. Unlike the LSM/YSZ/LSM$_{porous}$ cell, where the gas interacts with the porous LSM before reaching the sensing electrode, the test gas for the Pt/YSZ/Au cell interacts with only the porous YSZ electrolyte before reaching the dense Au sensing electrode. The porous YSZ may not be as catalytic for NO_x equilibration as the porous LSM and so a non-equilibrium composition is present at the electrode.

To understand the role of the YSZ electrolyte in the Pt/YSZ/Au cell, the effect of adding subsequent layers of porous YSZ electrolyte onto the Au wire electrodes was investigated (see Fig. 1a). Figure 9a shows the Nyquist plot for the Pt/YSZ/Au cell at 650°C with a single layer of YSZ electrolyte

on the surface of approximately 50 to 100 μm thickness. The addition of a second layer of YSZ electrolyte onto the Au wire electrodes, as shown in Fig. 9b, caused a decrease in the high-frequency (higher than about 10 kHz) impedance, where the cusp between the two arcs decreased by $\sim$500 Ω from $\sim$2500 to $\sim$2000 Ω. The decrease in high-frequency impedance indicates that the additional YSZ electrolyte increases the bulk oxygen ionic conductivity between the two electrodes.

The subsequent addition of a third and fourth layer of YSZ electrolyte (each layer was approximately 50 to 100 μm) did not cause any additional changes in the high-frequency impedance. Therefore, the current path for the bulk oxygen ionic conductivity between the Au wire electrode and Pt counter electrode is only influenced by the second layer of YSZ electrolyte, and additional layers do not provide further enhancements in ionic conductivity.

The low-frequency (less than about 1 kHz) impedance behavior was also affected by the addition of a second layer of YSZ electrolyte on the Au wire electrodes. In Figs. 9a and b, for 10.5% O_2, the diameter of the low-frequency arc, or electrode impedance, decreased by $\sim$1500 Ω with the addition of a second YSZ electrolyte layer, while the electrode impedance decreased by $\sim$1000 Ω and $\sim$1600 Ω for 10.5% O_2 with 100 ppm NO and for 10.5% O_2 with NO_2, respectively.

The decrease in electrode impedance indicates that the additional YSZ

electrolyte increased both the O_2 and NO_x reaction rates at the Au wire sensing electrode. However, the effect was more significant for NO_2 compared to NO. In Fig. 9a, the Pt/YSZ/Au cell with a single layer of YSZ electrolyte on the surface produced similar impedance responses with the addition of either 100 ppm NO or NO_2 to the 10.5% O_2 background gas. In Fig. 9b, with the addition of a second layer of YSZ electrolyte, the addition of NO_2 caused a larger decrease in electrode impedance than the addition of NO. The subsequent addition of a third and fourth layer of YSZ electrolyte (each layer was approximately 50 to 100 μm) did not cause any additional relative changes in the NO_2 vs. NO response (see Figs. 9c and 9d); however, the overall electrode impedance continued to decrease.

Figure 10 shows the corresponding I-V curves in 10.5% O_2 with and without 100 ppm of NO or NO_2 added for varying layers of YSZ electrolyte on the surface of the Pt/YSZ/Au cell. For all samples, OCP values ranging from -0.15 to +0.15 mV and -1.5 to -1 mV were measured for 10.5% O_2 and 10.5% O_2 with 100 ppm NO, respectively, which is similar to the I-V behavior noted for the LSM/YSZ/LSM_{porous} cell at 575°C shown in Fig. 8. However, in the case of NO_2, larger OCP values were measured. As shown in Fig. 10a, for the single layer of YSZ electrolyte, an OCP of approximately 10 mV was measured for 10.5% O_2 with 100 ppm NO_2. In Fig. 10b, with the addition of a second layer of YSZ electrolyte, the measured OCP with NO_2 present increased to approximately 19 mV. Further increases in the number

of YSZ layers, as shown in Figs. 10c and d, did not produce additional changes in the OCP behavior for NO_2 in the measured gas.

The results from varying the amount of YSZ electrolyte on the surface of the Pt/YSZ/Au cell indicate that porous YSZ may provide a more favorable pathway for NO_2, compared to NO, to the sensing interface. For thin layers of YSZ less than about 100 μm, there is limited interaction between the NO_x and the porous YSZ; all the gas introduced reaches the sensing interface without any changes in composition. If only the gas concentration (not electrode composition) influences the charge-transfer reaction (see Eq. 5) at the electrode/electrolyte interface and the resulting measured impedance, then additions of either NO or NO_2 would produce a similar response.

As the amount of surface YSZ electrolyte increases, the NO_x interacts more significantly before reaching the sensing interface. The NO_2 may have a faster diffusion pathway than NO on porous YSZ. However, as discussed previously, interaction with the YSZ electrolyte increases the O_2, NO, and NO_2 reaction rates. Therefore, the relative enhancement of NO_2 selectivity over NO likely occurs when a sufficient amount of YSZ is present to make surface interaction available, but increasing the amount of the YSZ electrolyte beyond a certain point may not provide any additional enhancement since both the NO_2 and NO reaction rates are being affected.

Previous results support our observation that NO_2 may have a faster diffusion path on the porous YSZ.[12] In earlier prototypes, spring-loaded

electrical contacts were used to contact the Au metal electrode to the porous YSZ. This was a geometry that minimized interaction between NO_x and the porous YSZ since the measured gas could reach the interface directly without interacting with other parts of the sensor, such as the case in this study where diffusion through porous YSZ was required. For this earlier prototype, almost identical impedance responses to NO and NO_2 were measured.[12]

Conclusions

Impedancemetric NO_x sensing has been investigated using Pt/YSZ/Au and LSM/YSZ/LSM_{porous} cells. Similar NO_x sensitivities to less than 5 ppm NO for both cells were observed, and response times (10-90% response/recovery) of less than 10 s. However, the LSM/YSZ/LSM_{porous} cell required operation at a lower temperature (575°C) compared to the Pt/YSZ/Au cell in order to achieve the same NO_x sensitivity. This is thought to be due to differing catalytic activity towards O_2 and NO_x.

Interaction of the test gas with the porous LSM counter electrode was found to affect the gas composition that was measured at the sensing electrode in the LSM cell. This interaction resulted in complete gas phase equilibration of NO_x and identical sensitivity towards NO and NO_2. Current-potential (I-V) curves that showed negligible, less than approximately 2 mV, open circuit potential (OCP) values and similar reaction rates at both electrodes support the hypothesis that similar gas phase compositions were

present at both electrodes.

In contrast, the NO_x selectivity for the cell with the Au sensing electrode varied depending on the cell design: increasing the amount of the porous YSZ electrolyte on the surface of the cell produced larger NO_2 sensitivity compared to NO. The I-V curves for the Au sensing electrode showed negligible OCP values for O_2 with and without NO, but showed large OCP values of 10 to 19 mV for O_2 with NO_2. Both the impedance and I-V behavior suggest that the porous YSZ may provide a more rapid diffusion pathway for NO_2 than NO. The relative enhancement of NO_2 selectivity over NO likely occurs when a sufficient amount of YSZ is present to make surface interaction available, but further increases in the amount of the YSZ electrolyte beyond a certain point may not provide any additional enhancement since both the NO_2 and NO reaction rates are being affected. Finally, the ability to measure NO_x in the presence of a large background of O_2 is likely due to a reaction pathway that is dominated by adsorption and diffusion on the YSZ electrolyte.

Acknowledgements

This work was performed under the auspices of the U.S. Department of Energy by Lawrence Livermore National Laboratory under Contract DE-AC52-07NA27344. Two of the coauthors (LYW and RSG) would like to acknowledge support from the DOE Office of Vehicle Technologies and the

Program Manager, Jerry Gibbs. We also gratefully acknowledge contributions from D. J. Kubinsky and R. E. Soltis, both from Ford Motor Company.

References

1. N. Yamazoe, *Sens. Actuators, B*, **108**, 2 (2005).

2. R. Moos, *Int. J. Appl. Ceram. Technol.*, **2**, 401 (2005).

3. S. Akbar, P. Dutta, and C. Lee, *Int. J. Appl. Ceram. Technol.*, **3**, 302 (2006).

4. F. Ménil, V. Coillard, and C. Lucat, *Sens. Actuators, B*, **67**, 1 (2000).

5. S. Zhuiykov and N. Miura, *Sens. Actuators, B*, **121**, 639 (2007)

6. J. W. Fergus, *Sens. Actuators, B*, **121**, 652 (2007)

7. S. -W. Song, L. P. Martin, R. S. Glass, E. P. Murray, J. H. Visser, R. E. Soltis, R. F. Novak, and D. J. Kubinski, *J. Electrochem. Soc.*, **153**, H171 (2006)

8. N. Miura, M. Nakatou, and S. Zhuiykov, *Ceram. Int.*, **30**, 1135 (2004).

9. N. Wu, Z. Chen, J. Xu, M. Chyu, and S.X. Mao, *Sens. Actuators, B*, **110**, 49 (2005).

10. N. Miura, T. Koga, M. Nakatou, P. Elumalai, and M. Hasei, *J. Electroceram.*, **17**, 979 (2006).

11. L. P. Martin, L. Y. Woo, and R. S. Glass, *J. Electrochem. Soc.*, **154**, J97 (2007).

12. L. Y. Woo, L. P. Martin, R. S. Glass, and R. J. Gorte, *J. Electrochem. Soc.*, **154**, J129 (2007).

13. L. Y. Woo, L. P. Martin, R. S. Glass, W. Wang, S. Jung, R. J. Gorte, E. P. Murray, R. F. Novak, and J. H. Visser, *J. Electrochem. Soc.*, **155**, J32 (2008).

14. J. R. Macdonald, *Impedance Spectroscopy: Emphasizing Solid Materials and Systems*, p. 5, John Wiley & Sons, New York (1987).

15. J. -C. Yang and P. K. Dutta, *J. Phys. Chem. C*, **111**, 8307 (2007).

16. V. V. Popovskii, *Theor. Exp. Chem.*, **5**, 688 (1969).

17. Y. D. Pankratiev, *React. Kinet. Catal. Lett.*, **20**, 255 (1982).

18. K. -S. Song, H. X. Cui, S. D. Kim, and S. -K. Kang, *Catal. Today*, **47**, 155 (1999).

19. B. Morel, R. Roberge, S. Savoie, T. W. Napporn, and M. Meunier, *Appl. Catal., A*, **323**, 181 (2007).

20. E. D. Wachsman, in *Solid-State Ionic Devices III*, E. D. Wachsman, K. Swider-Lyons, M. F. Carolan, F. H. Garzon, M. Liu, and J. R. Stetter, Editors, PV 2002-26, p. 215, The Electrochemical Society Proceedings Series, Pennington, NJ (2003).

21. E. Di Bartolomeo, M. L. Grilli, and E. Traversa, *J. Electrochem. Soc.*, **151**, H133 (2004).

List of Figures

in 10.5% O_2 and in 10.5% O_2 with 100 ppm NO or 100 ppm NO_2.

Fig. 9: Nyquist plots of Pt/YSZ/Au cell at 650°C in 10.5% O_2 and in 10.5% O_2 with 100 ppm NO or 100 ppm NO_2 and varying amounts of YSZ surface layers: (a) one layer, (b) two layers, (c) three layers, and (d) four layers. Numbers corresponding to darkened points represent log of frequency in Hz

Fig. 10: Current-potential (I-V) curves of Pt/YSZ/Au cell at 650°C in 10.5% O_2 and in 10.5% O_2 with 100 ppm NO or 100 ppm NO_2 and varying amounts of YSZ surface layers: (a) one layer, (b) two layers, (c) three layers, and (d) four layers.

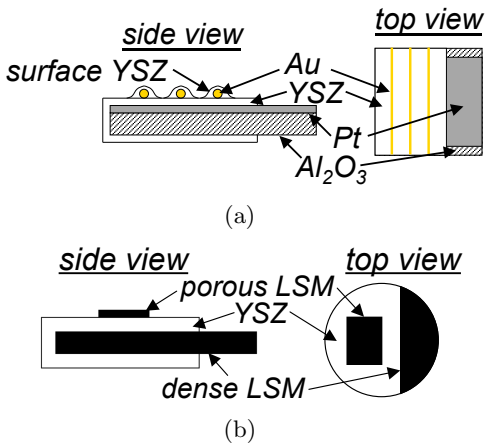

Figure 1: Schematic of (a) Pt/YSZ/Au and (b) LSM/YSZ/LSM$_{porous}$ cells.

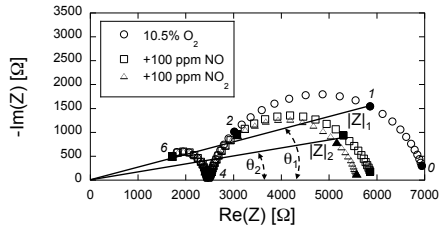

Figure 2: Nyquist plot of Pt/YSZ/Au cell at 650°C in 10.5% O_2 and in 10.5% O_2 with 100 ppm NO or 100 ppm NO_2. $|Z|$ and θ at 10 Hz are shown as solid and dotted lines, respectively, where $|Z|_1$ and θ_1 refer to the response in 10.5% O_2 and $|Z|_2$ and θ_2 refer to the response in 10.5% O_2 with 100 ppm of NO or 100 ppm NO_2. Numbers corresponding to darkened points represent log of frequency in Hz.

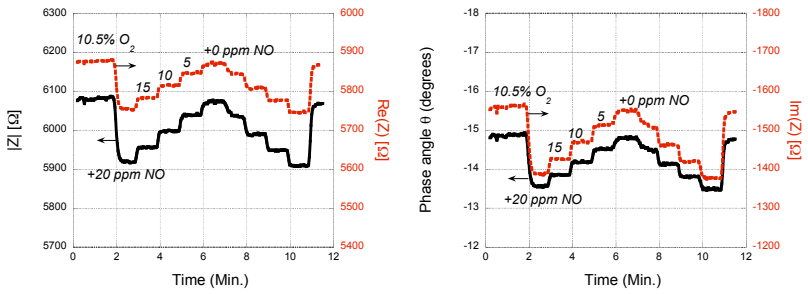

(a) (b)

Figure 3: Response of Pt/YSZ/Au cell at 650°C and 10 Hz using (a) modulus ($|Z|$) and real impedance ($\mathrm{Re}(Z)$) and (b) phase angle (θ) and imaginary impedance ($\mathrm{Im}(Z)$) as the NO_x sensing signal.

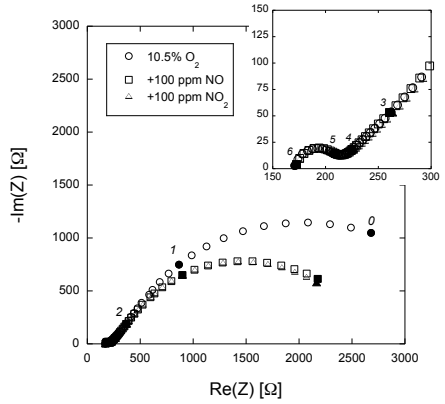

Figure 4: Nyquist plot of LSM/YSZ/LSM$_{porous}$ cell at 575°C in 10.5% O_2 and in 10.5% O_2 with 100 ppm NO or 100 ppm NO_2. Numbers corresponding to darkened points represent log of frequency in Hz.

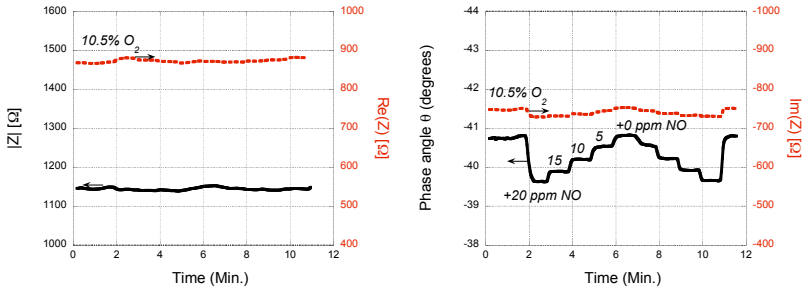

(a) (b)

Figure 5: Response of Pt/YSZ/Au cell at 650°C and 10 Hz using (a) modulus ($|Z|$) and real impedance ($\mathrm{Re}(Z)$) and (b) phase angle (θ) and imaginary impedance ($\mathrm{Im}(Z)$) as the NO_x sensing signal.

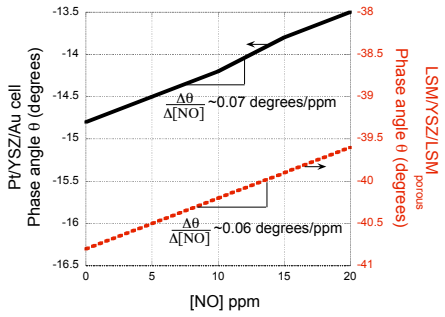

Figure 6: Phase angle signal vs. concentration of NO (ppm) for the Pt/YSZ/Au and LSM/YSZ/LSM$_{porous}$ cells.

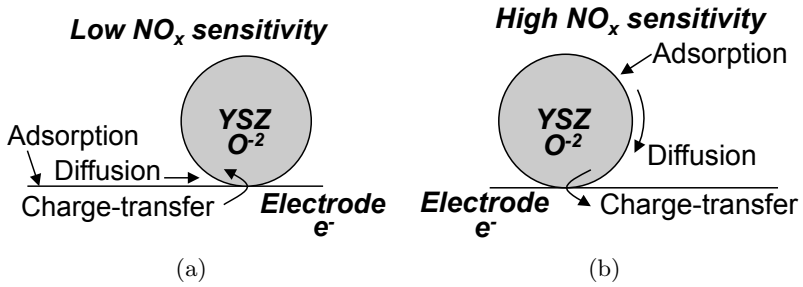

Figure 7: Illustration of simplified steps involved in impedancemetric NO_x sensing for (a) low NO_x sensitivity and (b) high NO_x sensitivity.

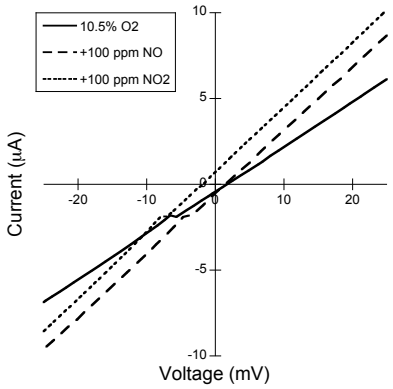

Figure 8: Current-potential (I-V) curve of LSM/YSZ/LSM$_{porous}$ cell at 575°C in 10.5% O_2 and in 10.5% O_2 with 100 ppm NO or 100 ppm NO_2.

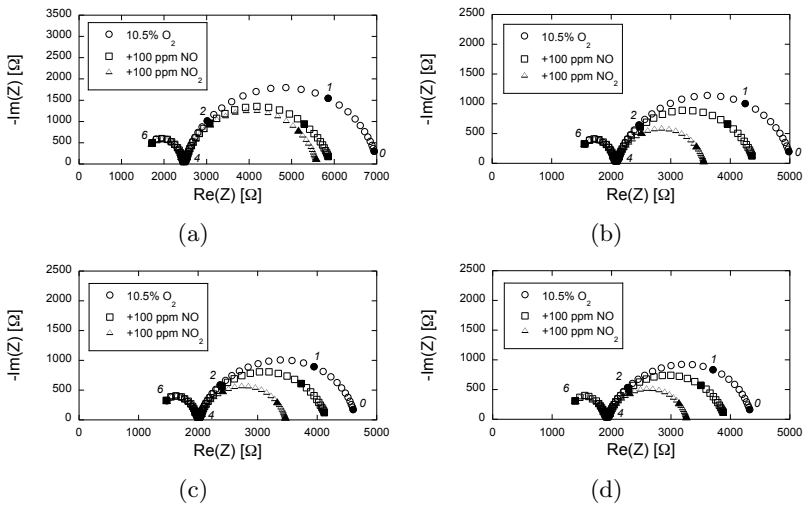

Figure 9: Nyquist plots of Pt/YSZ/Au cell at 650°C in 10.5% O_2 and in 10.5% O_2 with 100 ppm NO or 100 ppm NO_2 and varying amounts of YSZ surface layers: (a) one layer, (b) two layers, (c) three layers, and (d) four layers. Numbers corresponding to darkened points represent log of frequency in Hz.

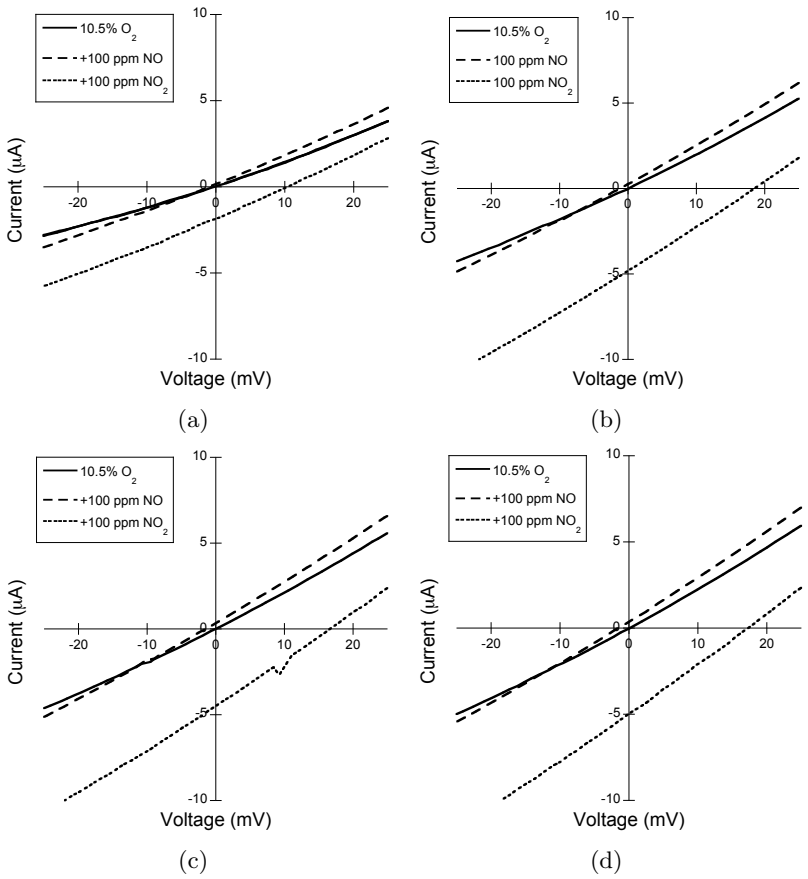

Figure 10: Current-potential (I-V) curves of Pt/YSZ/Au cell at 650°C in 10.5% O_2 and in 10.5% O_2 with 100 ppm NO or 100 ppm NO_2 and varying amounts of YSZ surface layers: (a) one layer, (b) two layers, (c) three layers, and (d) four layers.